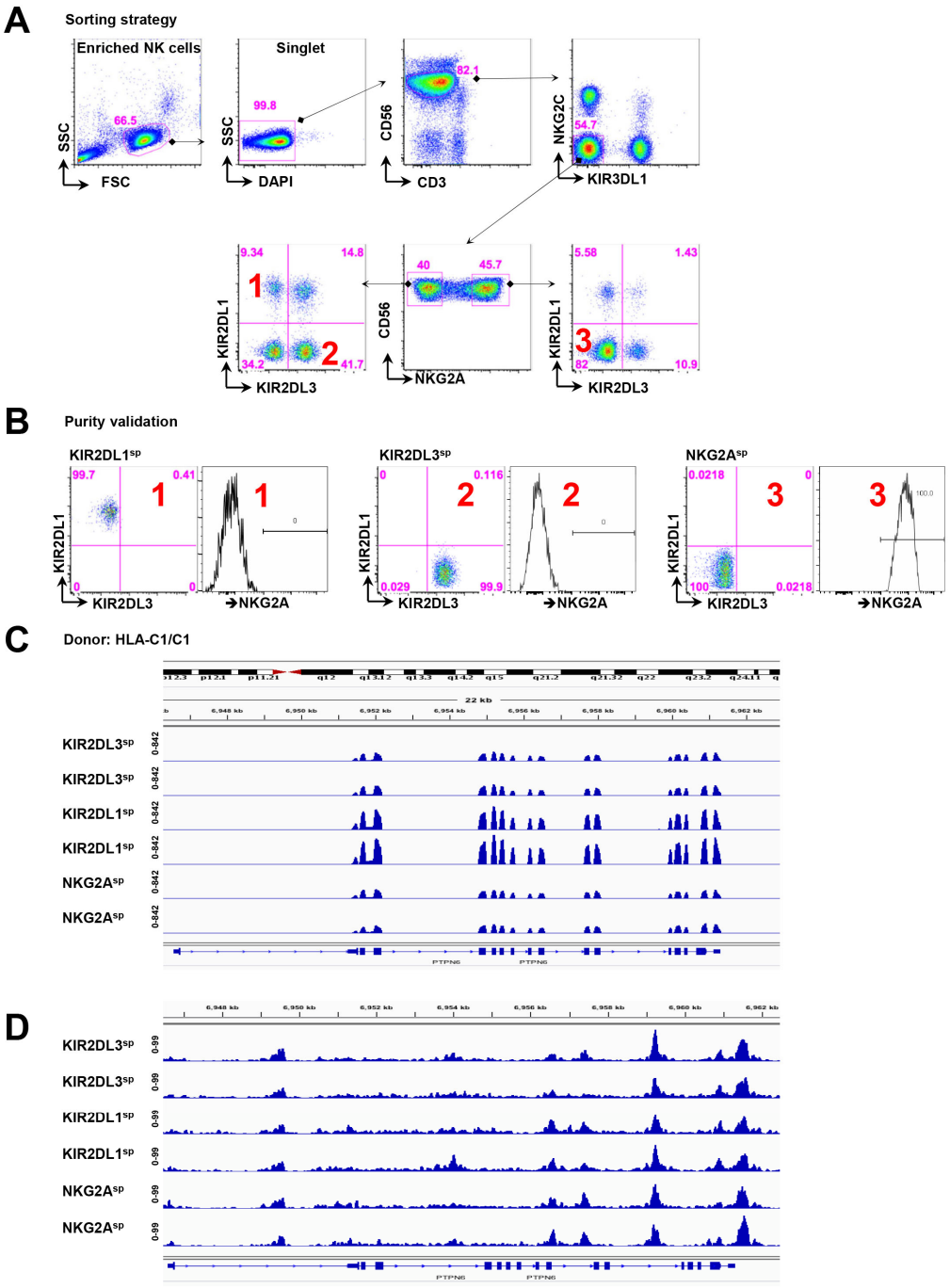

Fig. S1. Sorting strategy of human NK cell subsets. (**A**) NK cells were enriched from freshly isolated PBMCs by negative selection. $CD3^{-}CD56^{dim}$ NK cells were sorted from live cells. The NKG2C- and KIR3DL1-positive NK cells were excluded. KIR2DL1sp, KIR2DL3sp, and NKG2Asp NK cells were sorted. (**B**) Purity validation of the indicated sorted NK cell subsets. (**C**) Genomic tracks of mapped RNA-seq reads at the *PTPN6* loci from the sorted populations. Technical duplicates are indicated. KIR2DL3 vs. KIR2DL1: $P = 0.01$; NKG2A vs. KIR2DL1: $P = 0.006$. (**D**) Genomic tracks of mapped ATAC-seq reads at the *PTPN6* loci from sorted NK cell populations. Technical duplicates are indicated. KIR2DL3 vs. KIR2DL1: $P = 0.92$; NKG2A vs. KIR2DL1: $P = 0.17$.

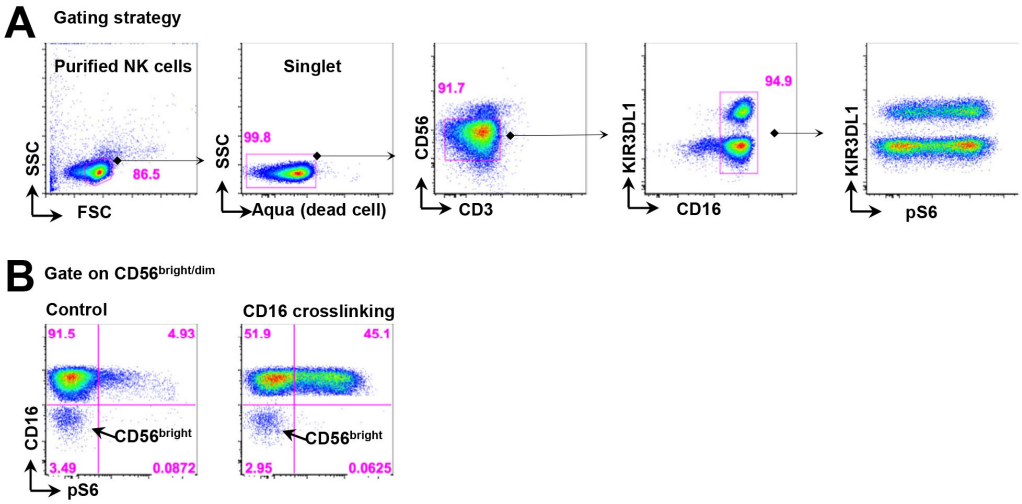

Fig. S2. Analysis strategy of anti-CD16 antibody crosslinking. (**A**) Freshly purified NK cells were labeled with Live-Dead Aqua and stimulated with biotinylated anti-CD16 and avidin for 5 min. Cells were then fixed and stained for CD3, CD56, KIR3DL1, and CD16. CD16-positive NK cells were gated to evaluate the percentage that were positive for pS6. (**B**) Purified NK cells stimulated with anti-IgG1 or crosslinking anti-CD16 antibody. The relative percentages of pS6-positive cells among CD16-positive and CD16-negative NK cells are shown. Plots are representative at least of five independent experiments.

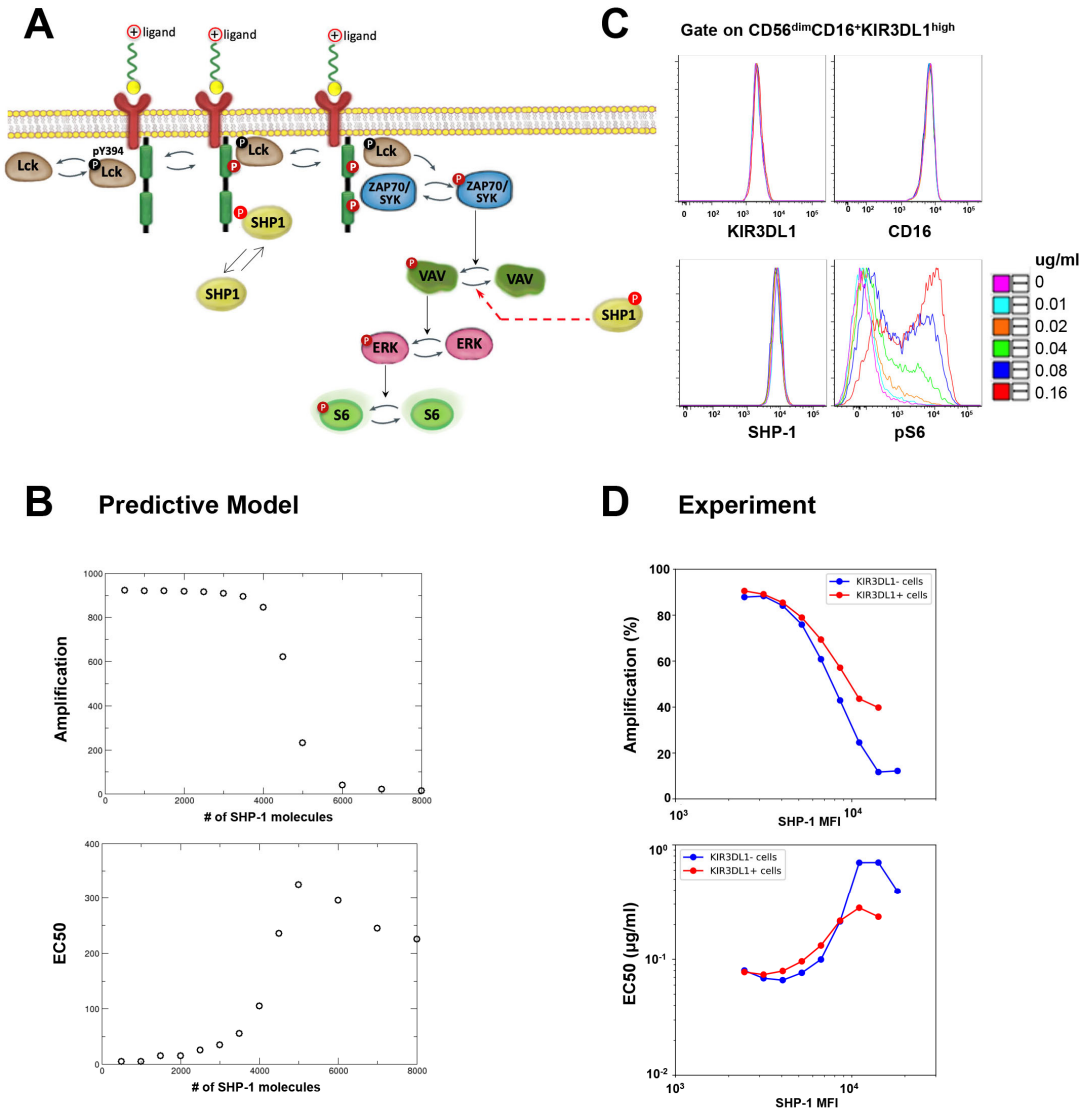

Fig. S3. Computational simulation of NK cell activation. (**A**) The signaling network used in the model. Fully activated activating receptors recruit Zap70 and Syk molecules, and receptor-bound Zap70 and Syk become phosphorylated by the action of Src family kinases (represented by Lck). Vav molecules are activated by phosphorylated Zap70 and Syk, and ERK molecules are activated by phosphorylated Vav in a coarse-grained, single-reaction step. Activated molecules are indicated by small circles with a symbol P. SHP-1 is recruited to the activating NK cell receptor signaling complex by the partially and fully phosphorylated ITAMs of the activating NK cell receptors. The ITAM-bound SHP-1 dephosphorylates pVav. (**B**) EC_{50} values and amplification of S6 phosphorylation upon varying the number of SHP-1 molecules in the simulation. (**C**) Analysis of KIR3DL1, CD16, SHP-1, and pS6 among $CD56^{dim}$ NK cells after incubation with the indicated amounts of crosslinking anti-CD16 antibodies. (**D**) Amplification and EC_{50} values of $KIR3DL1^{+}$ and $KIR3DL1^{-}$ NK cells after incubation with crosslinking anti-CD16 antibodies. Data are representative of two independent experiments.

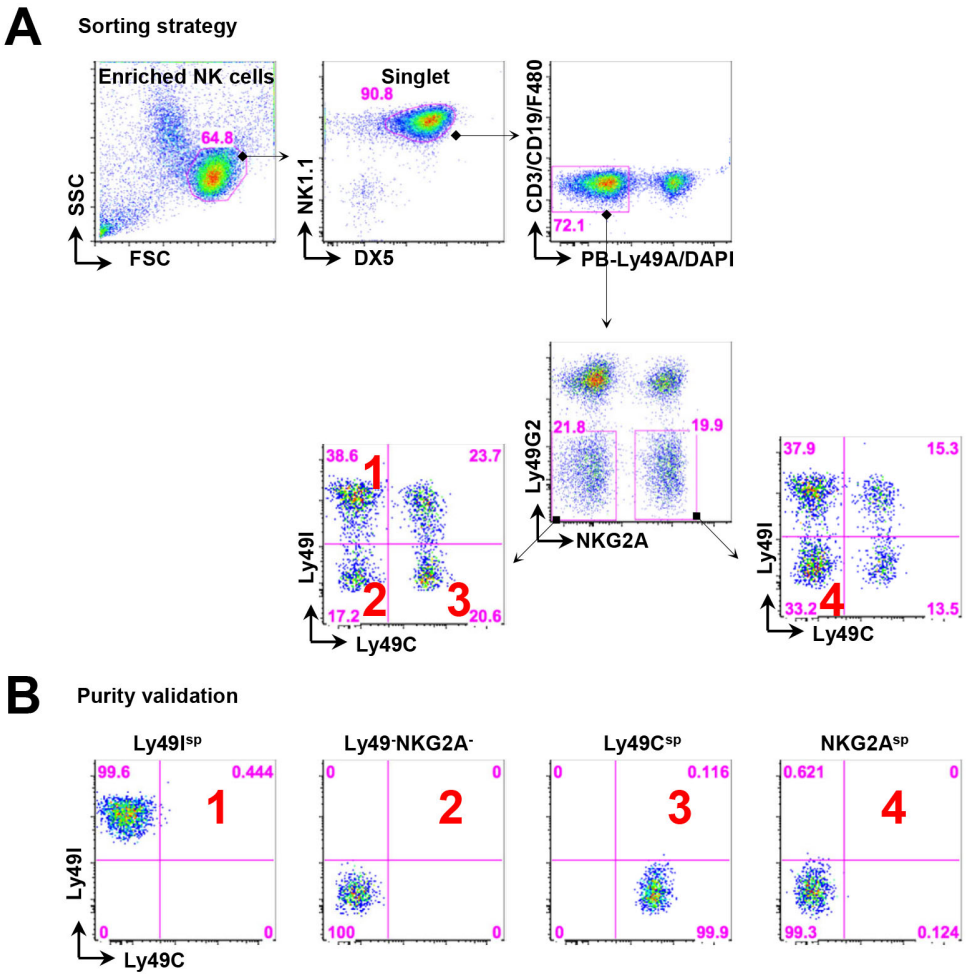

Fig. S4. Sorting strategy of NK cell subsets from B6 mice. (**A**) NK cells were enriched by negative selection from freshly prepared splenocytes. NK1.1^{+}DX5^{+}CD3^{-}CD19^{-}F480^{-} NK cells were sorted from live cells. The Ly49A- and Ly49G2-positive NK cells were excluded. Ly49Isp, Ly49Csp, and NKG2Asp NK cells were sorted, as numerically labeled. (**B**) Purity validation of the indicated sorted NK cell subsets.

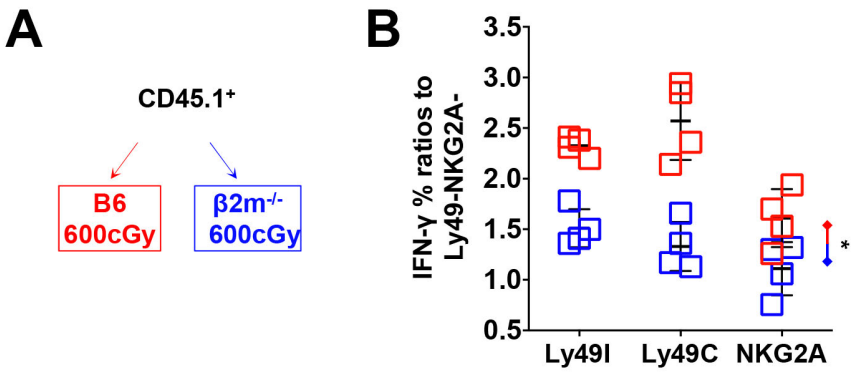

Fig. S5. NK cells reset responsiveness among distinct MHC-I environments. (**A**) CD45.1$^+$ splenocytes were transferred to irradiated B6 or β2m$^{-/-}$ recipient mice. (**B**) Analysis of the percentage of IFN-γ–positive cells among the transferred CD45.1$^+$ NK cell subsets after stimulation with anti-NK1.1 antibody. Data in (B) are means ± SD; n = 8 mice. *$P < 0.05$; **$P < 0.01$; ***$P < 0.001$; Friedman test and post hoc pairwise Wilcoxon test for multi-group comparison were used. Each symbol represents an individual mouse.

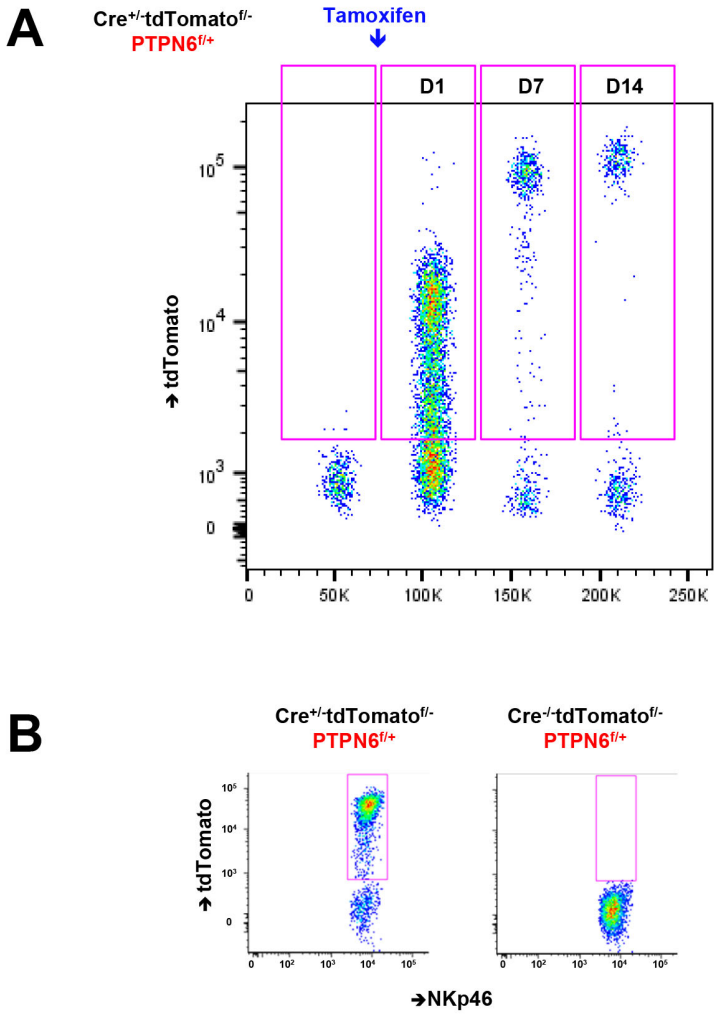

Fig. S6. TdTomato expression in NK cells after tamoxifen administration. (**A**) TdTomato expression among NKp46^{+} NK cells from CreERT2$^{+/-}$Ptpn6$^{fl/+}$tdtomato$^{fl/-}$ mice before and after tamoxifen administration. TdTomato expression profiles were concatenated into a single flow cytometry plot. Results are representative of two independent experiments. (**B**) TdTomato expression among NKp46^{+} splenic NK cells from CreERT2$^{+/-}$Ptpn6$^{fl/+}$tdtomato$^{fl/-}$ and CreERT2$^{-/-}$Ptpn6$^{fl/+}$tdtomato$^{fl/-}$ mice 3 days after tamoxifen administration. Data are representative of at least three independent experiments.

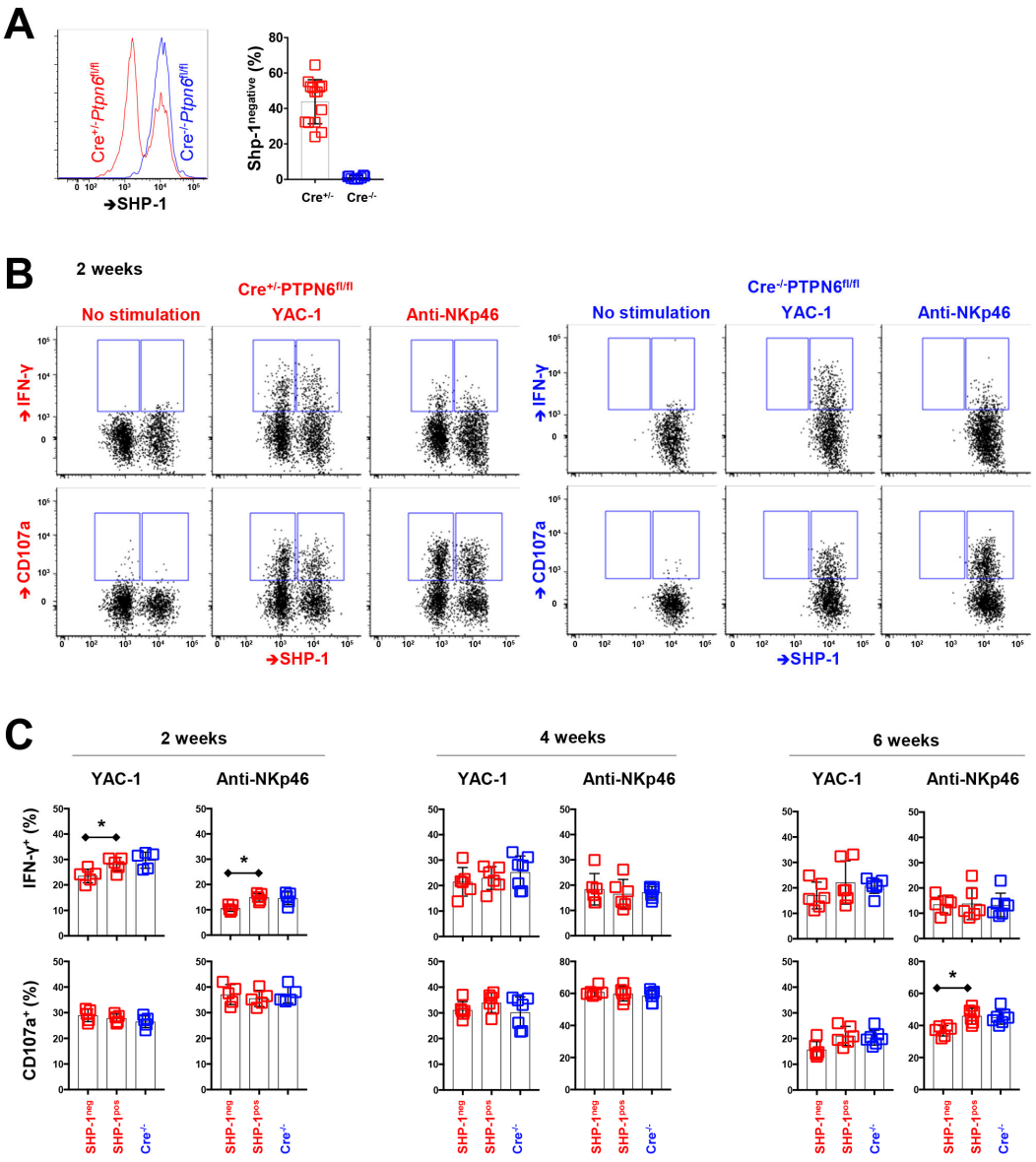

Fig. S7. Activity of SHP-1–negative NK cells. (**A**) SHP-1 expression among splenic NK cells from CreERT2$^{+/-}$Ptpn6$^{fl/fl}$ and CreERT2$^{-/-}$Ptpn6$^{fl/fl}$ mice 14 days after tamoxifen administration. (**B**) Representative plots demonstrating the frequency of IFN-γ production and CD107a mobilization among SHP-1^{+} and SHP-1^{-} NK cells after co-culture with YAC-1 cells or incubation with crosslinking anti-NKp46 antibodies at 2 weeks after the administration of tamoxifen to CreERT2$^{+/-}$Ptpn6$^{fl/fl}$ mice (red) and CreERT2$^{-/-}$Ptpn6$^{fl/fl}$ littermate control mice (blue). (**C**) Analysis of IFN-γ production and CD107a mobilization in SHP-1^{+} and SHP-1^{-} NK cells at 2, 4, and 6 weeks after the administration of tamoxifen to CreERT2$^{+/-}$Ptpn6$^{fl/fl}$ mice (red) and CreERT2$^{-/-}$Ptpn6$^{fl/fl}$ littermate control mice (blue). Results are pooled from two independent experiments. Data in (C) are means ± SD; n = 6 mice for each time point. *$P < 0.05$; **$P < 0.01$; ***$P < 0.001$; Friedman test and post hoc pairwise Wilcoxon test for multi-group comparison were used. Each symbol represents an individual mouse.

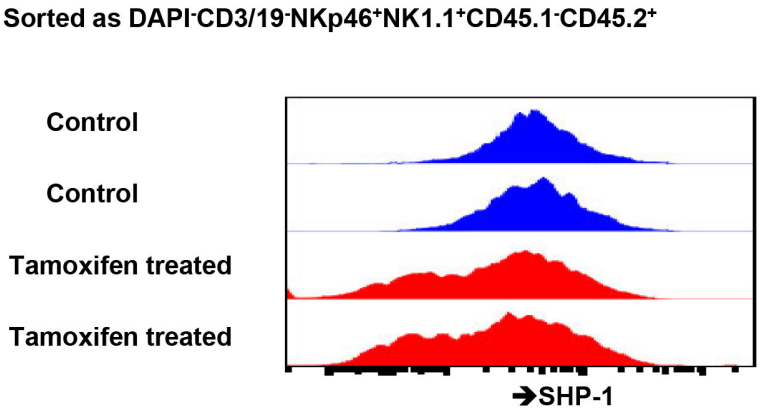

Fig. S8. SHP-1 expression among NK cells from chimeric animals. Mixed bone marrow chimeric mice were established as described in Fig. 5B. SHP-1 expression was evaluated among splenic $CD45.1^{-}CD45.2^{+}$ NK cells from chimeric animals that did or did not receive tamoxifen for 2 weeks. NK cells were sorted as $DAPI^{-}CD3^{-}CD19^{-}NKp46^{+}NK1.1^{+}CD45.1^{-}CD45.2^{+}$ for RNA-seq analysis. Only one sorting experiment was performed to prepare samples for RNA-seq. Two biological replicates were analyzed for each condition.

Table S1. Antibodies used in this study.

Antigen	Antibody clone	Source
CD3 epsilon	UCHT1	BD Bioscience
CD107a	H4A3	BD Bioscience
KIR3DL1	DX9	BD Bioscience
CD16	3G8	BD Bioscience
CD122	Mik-β3	BD Bioscience
CD45	2D1	BD Bioscience
CD56	NKH-1	Beckman Coulter
KIR2DL2/L3/S2	GL183	Beckman Coulter
NKG2A	Z199	Beckman Coulter
KIR2DL1/S1	EB6	Miltenyi
NKG2A	REA110	Miltenyi
NKG2C	REA205	Miltenyi
KIR2DL1	REA284	Miltenyi
KIR2DL3	REA147	Miltenyi
NKG2C	134591	R&D Systems
KIR2DL1	143211	R&D Systems
KIR2DL3	180701	R&D Systems
SHP-1	Y476	Abcam
SHP-1	C-19 (Polyclonal)	Santa Cruz
pS6	D57.2.2E	Cell signaling
Donkey anti-rat IgG (H+L)	Polyclonal	Jackson Immunoresearch
Fab fragment Goat anti-mouse IgG (H+L)	Polyclonal	Jackson Immunoresearch
CD16/32	2.4G2	BD Bioscience
NKG2A/C/E	20d5	BD Bioscience
Ly49I	YLI-90	Miltenyi
Ki67	REA183	Miltenyi
Ly49G2	4D11	Thermo Fisher
NK1.1	PK136	Biolegend
CD49b	DX5	Biolegend
CD3	145-2C11	Biolegend
CD19	6D5	Biolegend
F4/80	BM8	Biolegend
CD45.1	A20	Biolegend
CD45.2	104	Biolegend
Ly49A	YE-1	Biolegend

IFN-γ	XMG1.2	Biolegend
CD27	LG.3A10	Biolegend
CD11b	M1/70	Biolegend
CD107a	1D4B	Biolegend
NKp46	29A1.4	Biolegend
CD8a	2.43	InVivoMab
CD4	GK1.5	InVivoMab
CD19	1D3	InVivoMab
Ter-119	TER-119	InVivoMab
Ly49C	4LO3311	Drs. S. Lemieux and W. Yokoyama (Washington University School of Medicine)